Scripta Materialia 145 (2018) 41–44

Contents lists available at ScienceDirect

Scripta Materialia

journal homepage: www.elsevier.com/locate/scriptamat

Regular article

Band engineering and tuning thermoelectric transport properties of *p*-type $Bi_{0.52}Sb_{1.48}Te_3$ by Pb doping for low-temperature power generation

Kwanlae Kim [a], Gwansik Kim [a], Hwijong Lee [a], Kyu Hyoung Lee [b,*], Wooyoung Lee [a,*]

[a] Department of Materials Science and Engineering, Yonsei University, Seoul 03722, South Korea
[b] Department of Nano Applied Engineering, Kangwon National University, Chuncheon 24341, South Korea

ARTICLE INFO

Article history:
Received 7 September 2017
Accepted 7 October 2017
Available online 13 October 2017

Keywords:
Thermoelectric materials
Spark plasma sintering
Thermal conductivity
Electrical properties
Point defects

ABSTRACT

Herein, we report the results of a systematic study on the effect of Pb doping on the thermoelectric transport properties of *p*-type BiSbTe alloys to validate its potential applications for low-temperature power generation. The maximum power factor (~4.4 mW m^{-1} K^{-2}) at 300 K was obtained using 0.31 at.% Pb-doped $Bi_{0.52}Sb_{1.48}Te_3$ and was found to originate from an enlarged density of states effective mass as a result of the band engineering effect. The maximum efficiency of thermoelectric power generation (η_{max}) could be enhanced by 150% at ΔT = 220 K when the Pb concentration was optimized.

Among renewable energy resources, thermoelectric power generation has been given renewed attention because of the increased societal need to efficiently use energy from waste heat sources. According to the estimated USA waste heat sources by temperature range, the annual total energy from such heat sources was estimated to be approximately 41×10^9 GJ [1]. In particular, 78% of these annual total heat sources were in the low-temperature range (<200 °C). Thus, significant research has been devoted to power generation devices using BiTe-based thermoelectric materials because of their high conversion efficiency at low temperatures [2–7].

The conversion efficiency of thermoelectric materials is typically represented by the dimensionless figure of merit $zT = \sigma S^2 T/\kappa_{tot}$, where σ is the electrical conductivity, S is the Seebeck coefficient, and κ_{tot} is the total thermal conductivity (κ_{tot}) at a given absolute temperature T. The zT values of commercialized BiTe-based materials are approximately 1.0 near room temperature. However, given the wide range of temperatures for waste heat sources, it is necessary to develop customized BiTe-based thermoelectric materials with high zT values to maximize the power generation efficiency at a given temperature range for waste heat sources. One promising route to tune the temperature for a peak zT is compositional tuning such as through substitutional doping.

The most commercialized BiTe-based materials are $Bi_{0.5}Sb_{1.5}Te_3$ and $Bi_2Te_{2.7}Se_{0.3}$ for *p*-type and n-type materials, respectively [8]. In BiSbTe alloys, the carrier concentration (n_c) and power factor (σS^2) are sensitively influenced by the compositional ratio between Bi_2Te_3 and Sb_2Te_3 [8]. In previous reports [9,10], large power factors (>3.5 mW m^{-1} K^{-2}) were found for $Bi_{0.4}Sb_{1.6}Te_3$ and $Bi_{0.52}Sb_{1.48}Te_3$, and intensive work was conducted to study the effect of doping on the thermoelectric properties of compositions near these two materials [11–16]. Interestingly, the power factor was increased and the maximum zT was shifted toward higher temperatures by the incorporation of Ag [11,16,17] or Cu [14,15,18] into BiSbTe alloys. This was because some elements such as Ag and Cu are effective acceptors in *p*-type BiSbTe alloys, suppressing the effect of bipolar conduction at higher temperatures.

Pb is another promising dopant for shifting the temperature for a peak zT toward higher temperatures, because the previous work by Lin et al. [19] showed that Pb works as an effective acceptor. In this previous work, n_c in *p*-type $Bi_{0.4}Sb_{1.6}Te_3$ was increased by Pb doping, clarifying the temperature shifting effect. However, it is believed that an excessive amount of Pb gives rise to a decreased zT in $Bi_{0.4}Sb_{1.6}Te_3$.

In the present work, we systematically investigated the doping effect of Pb on the thermoelectric properties of $Bi_{0.52}Sb_{1.48}Te_3$ by precisely controlling the Pb content. $Bi_{0.52}Sb_{1.48}Te_3$ was selected because the n_c in $Bi_{0.52}Sb_{1.48}Te_3$ is smaller than that in $Bi_{0.4}Sb_{1.6}Te_3$ [8]. Thus, the effect of an increased n_c on BiSbTe could be effectively explored. We found that the maximum power factor (~4.4 mW m^{-1} K^{-2}) at 300 K was

* Corresponding authors.
E-mail addresses: khlee2014@kangwon.ac.kr (K.H. Lee), wooyoung@yonsei.ac.kr (W. Lee).

https://doi.org/10.1016/j.scriptamat.2017.10.009
1359-6462/

generated from 0.31 at.% Pb-doped $Bi_{0.52}Sb_{1.48}Te_3$ and this increased power factor was induced by an enlarged density of states (DOS) effective mass resulting from the band engineering effect. The enhanced zT values of BiSbTe alloys could be attributed to simultaneous improvements in the carrier transport and phonon scattering by Pb doping. Finally, the enhanced thermoelectric conversion efficiencies of Pb-doped BiSbTe alloys for low-temperature waste heat sources were evaluated by estimating the maximum efficiency of thermoelectric power generation.

High-purity (>99.999%) Bi, Sb, Te, and Pb granules were weighed based on the intended compositions of $Bi_{0.52}Sb_{1.48-x}Pb_xTe_3$ ($x = 0$–0.01 (0.5 at.%)), and ingots were synthesized using a melt-solidification process. The granules were loaded into vacuum-sealed quartz tubes with 14 mm diameters, and then melted in a box furnace for 10 h at 1085 °C. The acquired ingots were pulverized using a mortar and pestle and sieved to obtain <53 μm diameter particles. The powders were compacted using a spark plasma sintering (SPS) technique to form polycrystalline bulks under 45 MPa at 480 °C for 3 min in vacuum.

An X-ray diffraction (XRD) (Ultima IV/ME 200DX, Rigaku, Japan) analysis with CuKα radiation was conducted to analyze the phases of the sintered bulk samples. The XRD data were further analyzed to study the microstructural evolutions using the whole powder pattern fitting (WPPF) refinement method in the Rigaku PDXL XRD analysis software. Surface analysis was performed using field emission scanning electron microscope (JEOL-7800F). To obtain the n_c and Hall mobility (μ_{Hall}), Hall effect measurements were performed in the van der Pauw configuration under a 1 T magnetic field, and the n_c and μ_{Hall} values were subsequently computed using a one-band model. The power factor consisting of σ and S was measured from 300 K to 520 K using the thermoelectric property measurement system (ZEM-3, ULVAC, Japan). The total thermal conductivity ($\kappa_{tot} = \rho_S C_p \lambda$, where ρ_s is the density, C_p is the heat capacity, and λ is the thermal diffusivity) was identified from measurements taken separately. The laser flash method (Netzsch LFA-457, Germany) was used to measure λ. Low-temperature (100 K–400 K) C_p values were measured using a Quantum Design PPMS (physical properties measurement system). The C_p values at $T > 270$ K of all samples were nearly constant at 0.186 J g^{-1} K^{-1}. Thus, 0.186 J g^{-1} K^{-1} was used as a constant C_p value within the temperature range (300 K–520 K). The measured ρ_s of the sintered samples was ~6.65 g cm^{-3}. Note that all the material properties required to calculate zT values were measured in the direction perpendicular to the SPS pressing direction.

Fig. S1 (Supplementary data) shows the X-ray diffraction patterns of the planes perpendicular to the pressing direction for the sintered $Bi_{0.52}Sb_{1.48-x}Pb_xTe_3$ ($x = 0$–0.01 (0.5 at.%)) bulks, as described in the schematic. All of the patterns are indexed with the targeted rhombohedral Sb_2Te_3 structure (space group $R\bar{3}m$). Most of the Pb atoms were effectively substituted into Sb sites. This was also confirmed by the calculation of lattice parameters a and c obtained from the WPPF refinement, as shown in Fig. S2 (Supplementary data). Both lattice parameters a and c increase with the increasing Pb concentration. The increases in lattice parameters a and c by the Pb doping can be explained by the fact that the ionic radius of Pb (133 pm) is larger than that of Sb (90 pm). Further details on the orientation degree [20] of the {00l}planes for each sintered sample are introduced in Fig. S1. It is noted that no secondary phases are observed in the SEM images (Fig. S3, Supplementary data), indicating that the complete single phase of Pb-doped BiSbTe was successfully fabricated.

To clarify the effect of Pb doping on the BiSbTe alloy, the thermoelectric transport properties of $Bi_{0.52}Sb_{1.48-x}Pb_xTe_3$ ($x = 0$–0.01 (0.5 at.%)) were measured, and the associated parameters were calculated. Fig. 1(a) shows the variation in σ as a function of temperature for the pristine and Pb-doped $Bi_{0.52}Sb_{1.48}Te_3$ with dopant concentrations of 0.06–0.5 at.%. First, it can also be clearly observed that σ systematically increases from approximately 6.8×10^4 S m^{-1} to 2.0×10^5 S m^{-1} at 300 K as the Pb concentration increases because of the acceptor-like

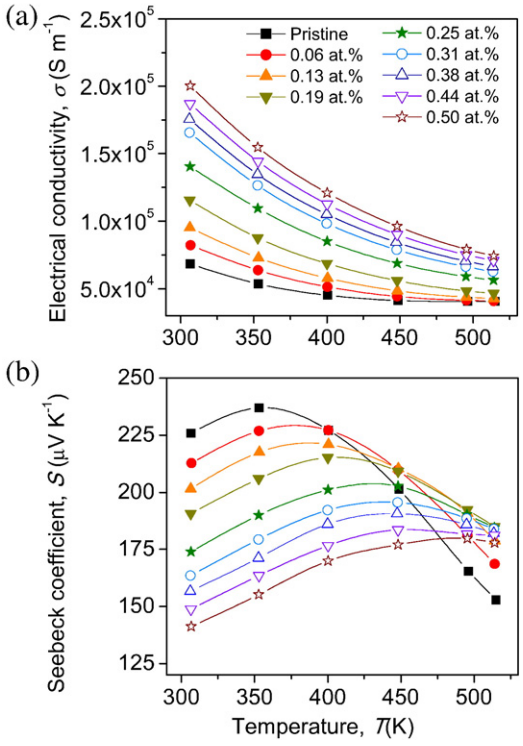

Fig. 1. Temperature dependences of (a) electrical conductivity and (b) Seebeck coefficient of $Bi_{0.52}Sb_{1.48-x}Pb_xTe_3$ ($x = 0$–0.01 (0.5 at.%)).

effect of the Pb atoms at Sb sites. To validate the increased σ by Pb doping, the n_c and μ_{Hall} values at 300 K were estimated from the Hall measurements, and are listed in Table S1 (Supplementary data). The n_c values gradually increased with increasing Pb concentration, while μ_{Hall} monotonically decreased after a 0.31 at.% Pb concentration ($Pb_{0.00625}Bi_{0.52}Sb_{1.47375}Te_3$). This implies that the enhancement of the power factor by Pb doping could be induced by the optimized n_c and μ_{Hall}.

The p-type behavior of Pb-doped BiSbTe alloys can be confirmed by the positive S in Fig. 1(b). In contrast to σ, at 300–350 K, S gradually decreased with an increase in the Pb concentration, which is reasonable because S is inversely proportional to n_c, according to [21].

$$S = \frac{8\pi^2 k_B^2}{3eh^2}\left(\frac{\pi}{3n_c}\right)^{2/3} m^* T, \quad (1)$$

where k_B, e, and h denote the Boltzmann constant, elementary charge, and Planck constant, respectively. The power factor was calculated from the measured σ and S, and is represented as a function of the temperature in Fig. 2(a). As the Pb concentration increases, a gradual increase in the power factor can be seen until a Pb concentration of 0.31 at.% at 300 K. After 0.31 at.%, the power factor at 300 K starts to decrease, while that near 500 K shows a monotonic increase until a 0.5 at.% Pb concentration. From Fig. 2(a), it is clarified that the maximum power factor of ~4.43 mW m^{-1} K^{-2} at 300 K can be obtained from a specific Pb concentration (0.31 at.%) via the optimized σ and S. It should be noted that the increase in the power factor is rather larger considering the trade-off relationship between σ and S, suggesting the band engineering effect by the Pb doping. To clarify this, we calculated the value of m_d^*, which is an important electronic transport parameter used to determine S. Fig. 2(b) shows S with respect to n_c for all the samples at 300 K, where the solid lines represent the equivalent m_d^* values for 0.7, 0.9, and 1.1 m_0, under the assumptions of a single parabolic band and an energy-independent carrier scattering approximation for degenerated semiconductors. As shown in Fig. 2(b), m_d^* increases with an increasing Pb concentration. Band engineering such as band flattening or Fermi level

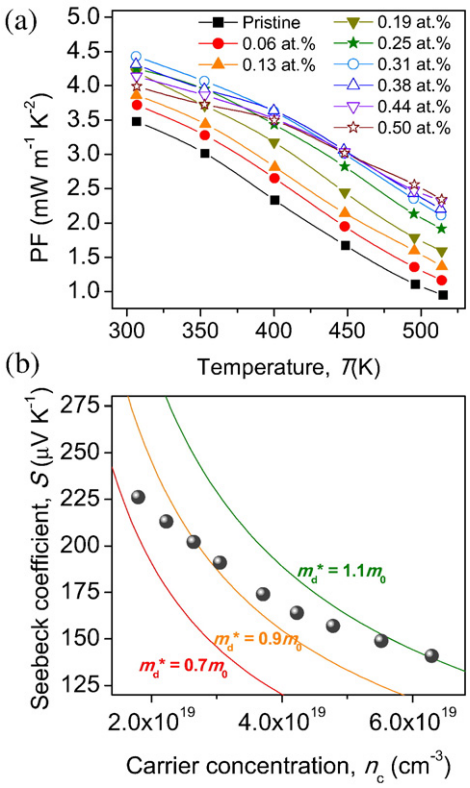

Fig. 2. (a) Temperature dependences of power factor of $Bi_{0.52}Sb_{1.48-x}Pb_xTe_3$ ($x = 0$–0.01 (0.5 at.%)) and (b) Seebeck coefficient as function of carrier concentration (Pisarenko plot) at 300 K for $Bi_{0.52}Sb_{1.48-x}Pb_xTe_3$ ($x = 0$–0.01 (0.5 at.%)).

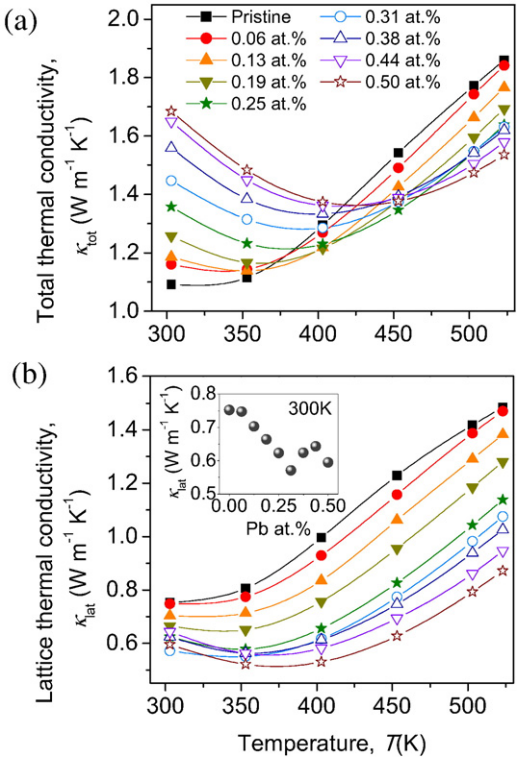

Fig. 3. Temperature dependences of (a) total thermal conductivity and (b) lattice thermal conductivity of $Bi_{0.52}Sb_{1.48-x}Pb_xTe_3$ ($x = 0$–0.01 (0.5 at.%)). The inset shows the lattice thermal conductivity (κ_{lat}) as a function of the Pb concentration at 300 K.

tuning may be the mechanism underlying the enhanced m_d^* by Pb doping [22,23].

Fig. 3(a) shows the temperature dependence of κ_{tot} for $Bi_{0.52}Sb_{1.48-x}Pb_xTe_3$ ($x = 0$–0.01 (0.5 at.%)). Two interesting effects of Pb doping can be clearly observed. First, at room temperature, κ_{tot} gradually increases from 1.09 W m^{-1} K^{-1} to 1.68 W m^{-1} K^{-1} with increasing Pb concentration, and second, the minimum κ_{tot} shifts toward higher temperatures from room temperature. The latter occurred because the onset of bipolar thermal conduction was suppressed by the increased concentration of the majority carriers (holes). To understand the increase in κ_{tot} by Pb doping at room temperature, the κ_{lat} value was calculated by subtracting κ_{ele} from κ_{tot}, where κ_{ele} was obtained using the Wiedemann–Franz law ($\kappa_{ele} = L\sigma T$, where L is the Lorenz number). The value of L was found using the following equation:

$$L = 1.5 + \exp\left[-\frac{|S|}{116}\right], \tag{2}$$

where L and S are in 10^{-8} W Ω K^{-2} and μV K^{-1}, respectively [24]. The resulting κ_{lat} with respect to temperature is shown in Fig. 3(b), which indicates that overall, κ_{lat} decreases with an increase in the Pb concentration over the entire temperature range. From Fig. 3(a) and (b), it is clarified that the enhancement in the κ_{tot} values of the BiSbTe alloys by Pb doping at a 300–350 K temperature range was induced not by κ_{lat} but by κ_{ele}. The variation in κ_{lat} with respect to the Pb concentration without the influence of the bipolar effect can be observed by comparing the κ_{lat} values at room temperature (inset in Fig. 3(b)). It can be seen that κ_{lat} is gradually decreased by Pb doping as a result of the intensified point defect phonon scattering from the mass difference between Pb ($M_{Pb} = 207.2$) and Sb ($M_{Sb} = 121.8$).

Fig. 4(a) shows the zT values of $Bi_{0.52}Sb_{1.48-x}Pb_xTe_3$ ($x = 0$–0.01 (0.5 at.%)) as a function of temperature. First, enhanced zT values over a wide temperature range (350–520 K) can be observed for the Pb-doped $Bi_{0.52}Sb_{1.48}Te_3$ (0.13–0.38 at.%) compared to pristine $Bi_{0.52}Sb_{1.48}Te_3$. Two distinct effects contributed to these enhanced zT values: (1) the increased power factor and (2) the shift in the minimum κ_{tot} toward higher temperatures. The significantly reduced κ_{tot} at 400–520 K was attributed to the suppression of the bipolar thermal conduction by the Pb incorporation, which controlled the majority carrier (hole) concentration. Hence, it was possible to maximize the zT value for the targeted waste heat temperature by selecting the optimal Pb concentration. As shown in Fig. 4(b), the most suitable doping level for the targeted temperature range can be identified based on the average zT (zT_{avg}). Overall, a higher zT_{avg} can be observed for 300–400 K compared to wider temperature ranges across a Pb concentration of 0–0.38 at.%. Fig. 4(b) also shows that a small zT_{avg} is unavoidable when the material is used at a wide range of temperatures such as 300–520 K. For the temperature ranges of 300–450 K, 300–500 K, and 300–520 K, a Pb concentration of 0.31 at.% provides the highest zT_{avg}.

The efficiency of the thermoelectric generation (η_{max}) based on Pb-doped $Bi_{0.52}Sb_{1.48}Te_3$ was estimated using the following equation:

$$\eta_{max} = \frac{\Delta T}{T_h}\frac{\sqrt{1+Z\cdot T_{avg}}-1}{\sqrt{1+Z\cdot T_{avg}}+\frac{T_c}{T_h}}, \tag{3}$$

where T_c and T_h are the cold-side and hot-side temperatures, respectively, and ΔT and T_{avg} are equal to $T_h - T_c$ and $(T_h + T_c)/2$, respectively [25]. Fig. 4(c) shows the computed η_{max} as a function of ΔT. Across the whole range of Pb concentrations, η_{max} shows an ascending trend until $\Delta T = 100$ K. However, the lightly Pb-doped samples (0.06–0.25 at.%) exhibit a descending trend after $\Delta T = 150$ K, while Pb concentrations of 0.38–0.5 at.% maintain an ascending trend until $\Delta T = 200$ K. Compared to the η_{max} value for pristine $Bi_{0.52}Sb_{1.48}Te_3$, a significant enhancement in η_{max} by Pb doping can be observed; η_{max} was enhanced by 39%, 73%, 131%, and 150% when $\Delta T = 100$ K, 150 K, 200 K, and 220 K,

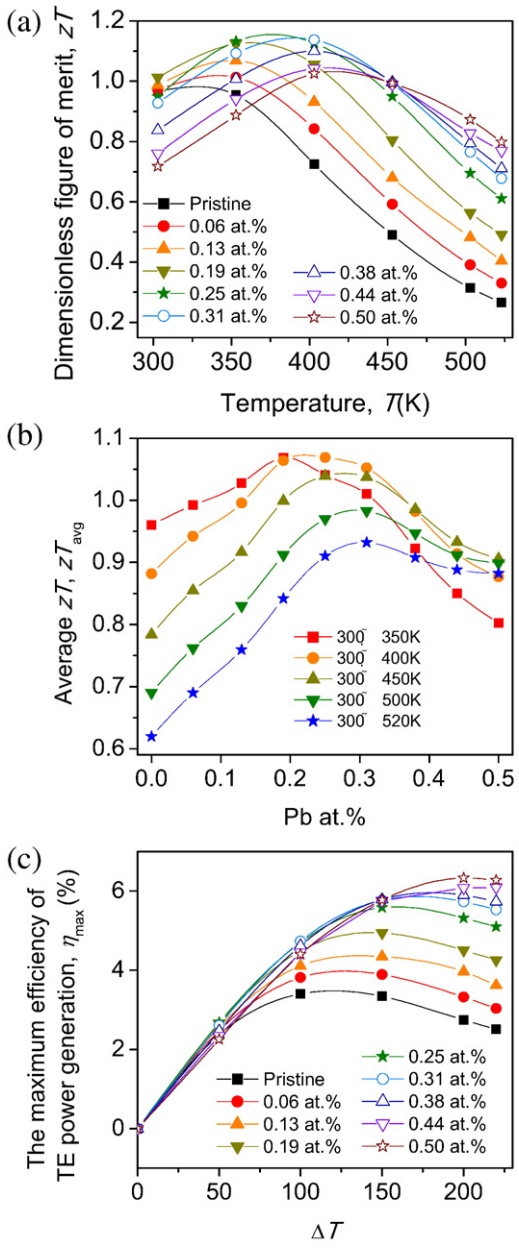

Fig. 4. (a) Dimensionless figure of merit zT as function of temperature (300–520 K). (b) Average zT values with respect to the Pb concentration for various ranges of temperature. (c) The maximum efficiency of thermoelectric power generation as a function of ΔT ($=T_h - T_c$).

respectively. zT was increased from 0.97 at 300 K to 1.14 at 400 K (an increase of ~18%) by the Pb doping, but η_{max} was significantly increased by up to 150%. This indicates that it is crucial to select the optimal doping level for high efficiency power generation.

We investigated the thermoelectric transport properties of $Bi_{0.52}Sb_{1.48-x}Pb_xTe_3$ (x = 0–0.01 (0.5 at.%)) polycrystalline bulks with precisely controlled Pb doping content to validate its potential application for low-temperature power generation. First, the power factors of BiSbTe in a temperature range of 300–520 K were enhanced by Pb doping as a result of an enlarged DOS effective mass induced by the band engineering effect, and the maximum power factor at 300–450 K was observed for a Pb concentration of 0.31 at.%. Second, the increased majority carrier (hole) concentration by Pb doping suppressed the onset of bipolar thermal conduction, shifting the minimum thermal conductivity toward higher temperatures. Consequently, the peak zT of BiSbTe was enhanced and precisely controlled at higher temperatures by Pb doping. In particular, the highest average zT values for various temperature ranges (300–450 K, 300–500 K, and 300–520 K) were generated by a 0.31 at.% Pb concentration. The estimated efficiency of thermoelectric power generation (η_{max}) in BiSbTe compounds was enhanced by 150% through Pb doping when $\Delta T = 220$ K. Interactive plots directly visualizing the relationship between zT_{avg} and η_{max} were provided, enabling systematic material design for low-temperature power generation.

Acknowledgment

This work was supported by the National Research Foundation of Korea (NRF) Grant funded by the Korea government (MSIP) (2014R1A2A1A10053869) and the Priority Research Centers Program (2009-0093823).

Appendix A. Supplementary data

Supplementary data to this article can be found online at https://doi.org/10.1016/j.scriptamat.2017.10.009.

References

[1] A.S. Rattner, S. Garimella, Energy 36 (2011) 6172–6183.
[2] S.I. Kim, K.H. Lee, H.A. Mun, H.S. Kim, S.W. Hwang, J.W. Roh, D.J. Yang, W.H. Shin, X.S. Li, Y.H. Lee, G.J. Snyder, S.W. Kim, Science 348 (2015) 109–114.
[3] L. Hu, T. Zhu, X. Liu, X. Zhao, Adv. Funct. Mater. 24 (2014) 5211–5218.
[4] H. Mun, S.M. Choi, K.H. Lee, S.W. Kim, ChemSusChem 8 (2015) 2312–2326.
[5] B. Poudel, Q. Hao, Y. Ma, Y. Lan, A. Minnich, B. Yu, X. Yan, D. Wang, A. Muto, D. Vashaee, X. Chen, J. Liu, M.S. Dresselhaus, G. Chen, Z. Ren, Science 320 (2008) 634–638.
[6] W. Xie, J. He, H.J. Kang, X. Tang, S. Zhu, M. Laver, S. Wang, J.R.D. Copley, C.M. Brown, Q. Zhang, T.M. Tritt, Nano Lett. 10 (2010) 3283–3289.
[7] K.T. Kim, S.Y. Choi, E.H. Shin, K.S. Moon, H.Y. Koo, G.-G. Lee, G.H. Ha, Carbon 52 (2013) 541–549.
[8] W. Xie, S. Wang, S. Zhu, J. He, X. Tang, Q. Zhang, T.M. Tritt, J. Mater. Sci. 48 (2013) 2745–2760.
[9] W. Xie, X. Tang, Y. Yan, Q. Zhang, T.M. Tritt, Appl. Phys. Lett. 94 (2009) 102111.
[10] K.H. Lee, S. Hwang, B. Ryu, K. Ahn, J. Roh, D. Yang, S.M. Lee, H. Kim, S.I. Kim, J. Electron. Mater. 42 (2013) 1617–1621.
[11] J.K. Lee, S.D. Park, B.S. Kim, M.W. Oh, S.H. Cho, B.K. Min, H.W. Lee, M.H. Kim, Electron. Mater. Lett. 6 (2010) 201–207.
[12] H. Mun, K.H. Lee, S.J. Kim, J.Y. Kim, J.H. Lee, J.H. Lim, H.J. Park, J.W. Roh, S.W. Kim, Materials 8 (2015) 959–965.
[13] K.H. Lee, S.M. Choi, J.W. Roh, S. Hwang, S.I. Kim, W.H. Shin, H.J. Park, J.H. Lee, S.W. Kim, D.J. Yang, J. Electron. Mater. 44 (2015) 1531–1535.
[14] Z. Huang, X. Dai, Y. Yu, C. Zhou, F. Zu, Scr. Mater. 118 (2016) 19–23.
[15] J.L. Cui, H.F. Xue, W.J. Xiu, W. Yang, X.B. Xu, Scr. Mater. 55 (2006) 371–374.
[16] J.L. Cui, H.F. Xue, W.J. Xiu, Mater. Lett. 60 (2006) 3669–3672.
[17] S. Seo, K. Lee, Y. Jeong, M.-W. Oh, B. Yoo, J. Phys. Chem. C 119 (2015) 18038–18045.
[18] Y.S. Lim, M. Song, S. Lee, T.H. An, C. Park, W.S. Seo, J. Alloys Compd. 687 (2016) 320–325.
[19] C.C. Lin, D. Ginting, R. Lydia, M.H. Lee, J.S. Rhyee, J. Alloys Compd. 671 (2016) 538–544.
[20] F.K. Lotgering, J. Inorg. Nucl. Chem. 9 (1959) 113–123.
[21] G.J. Snyder, E.S. Toberer, Nat. Mater. 7 (2008) 105–114.
[22] G. Tan, L.D. Zhao, M.G. Kanatzidis, Chem. Rev. 116 (2016) 12123–12149.
[23] Y. Pei, H. Wang, G.J. Snyder, Adv. Mater. 24 (2012) 6125–6135.
[24] H.S. Kim, Z.M. Gibbs, Y. Tang, H. Wang, G.J. Snyder, APL Mater. 3 (2015) 41506.
[25] A.F. Ioffe, Semiconductor Thermoelements, and Thermoelectric Cooling, Infosearch, London, 1957.